1-23-2013

Membrane Association via an N-terminal Amphipathic Helix is Required for the Cellular Organization and Function of RNase II

Feng Lu
University of Connecticut School of Medicine and Dentistry

Aziz Taghbalout
University of Connecticut School of Medicine and Dentistry

JBC Papers in Press. Published on January 23, 2013 as Manuscript M112.408674
The latest version is at http://www.jbc.org/cgi/doi/10.1074/jbc.M112.408674

Membrane association via an N-terminal amphipathic helix is required for the cellular organization and function of RNase II*

Feng Lu and Aziz Taghbalout

Department of Molecular, Microbial, and Structural Biology, University of Connecticut Health Center, 263 Farmington Avenue, Farmington, CT, 06032, USA

*Running title: Cellular organization of RNase II

To whom correspondence should be addressed: Aziz Taghbalout, Department of Molecular, Microbial, and Structural Biology, University of Connecticut Health Center, 263 Farmington Avenue, Farmington, CT, 06032, USA. Tel.: (860) 679-4208; Fax: (860) 679-1239, Email: taghbalout@neuron.uchc.edu

Keywords: RNase II; Amphipathic membrane binding domain; Cellular organization; Cellular compartmentalization; RNA processing and degradation; Bacterial cytoskeleton.

Background: Cellular organization of the *Escherichia coli* exoribonuclease RNase II is unknown.
Results: Membrane association and self-interactions are both required for the RNase II cellular organization.
Conclusion: Membrane binding facilitates RNase II interactions leading to assembly into organized cellular structures.
Significance: Interplay of membrane association and formation of organized membrane-associated cellular structures could provide a mechanism to organize multiprotein systems within the bacterial cell.

SUMMARY

The subcellular localization of the exoribonuclease RNase II is not known despite the advanced biochemical characterization of the enzyme. Here we report that RNase II is organized into cellular structures that appear to coil around the *Escherichia coli* cell periphery and that RNase II is associated with the cytoplasmic membrane by its amino-terminal amphipathic helix. The helix also acts as an autonomous transplantable membrane-binding domain capable of directing normally cytoplasmic proteins to the membrane. Assembly of the organized cellular structures of RNase II required the RNase II amphipathic membrane-binding domain. Co-immunoprecipitation of the protein from cell extracts indicated that RNase II interacts with itself. The RNase II self-interaction and the ability of the protein to assemble into organized cellular structures required the membrane-binding domain. The ability of RNase II to maintain cell viability in the absence of the exoribonuclease PNPase was markedly diminished when the RNase II cellular structures were lost due to changes in the amphipathicity of the N-terminal helix, suggesting that membrane association and assembly of RNase II into organized cellular structures play an important role in the normal function of the protein within the bacterial cell.

Bacterial RNA processing and degradation is an essential cellular function whose maintenance requires the coordinated action of a large number of ribonucleases and other proteins. Amongst these, RNase II, the 644 amino acid product of the *Escherichia coli rnb* gene, is a processive hydrolytic exoribonuclease that acts on the 3' end of single-stranded RNA, leading to formation of 5' mononucleotides and a short 5' terminal oligonucleotide (1). In *E. coli*, RNase II accounts for about 90% of the total exoribonucleolytic activity of cell extracts (2). The primary role of RNase II appears to be the degradation of mRNA (3), although in the absence of other exoribonucleases, RNase II also functions in the processing of tRNA and other stable RNAs (4,5).

Although the subcellular location of RNase II is not known, the protein is generally regarded as a

soluble protein. Here we show that RNase II is a membrane-associated protein that binds the cytoplasmic membrane via an amino-terminal amphipathic alpha-helix. Fluorescence localization studies showed that RNase II is organized within the cell as membrane-associated ordered structures. Membrane binding of RNase II is required for assembly of the RNase II organized cellular structures, and membrane binding is also required for the self-interaction of RNase II in cell extracts. Assembly of the RNase II cellular structures is required for the normal growth of cells that lack the exoribonuclease PNPase, suggesting an important role of the RNase II higher order cellular organization for the normal function of the cell. The functional implications of the membrane association in the assembly of the organized cellular structures of RNase II and in the associated cell functions of the protein are discussed.

EXPERIMENTAL PROCEDURES

Strains, plasmids and growth conditions- E. coli strains were grown in LB medium (6) to which 100 µg/ml ampicillin, 30 µg/ml kanamycin, 30 µg/ml chloramphenicol, or 0.4% (w/v) glucose were added when indicated. Plasmids and strains are listed in Table 1 and the details of their construction are available upon request. Gene knockouts and *yfp* fusion to the chromosomal *rnb* gene were constructed by linear DNA recombination using λ Red-mediated gene replacement (7). HA and Flag-epitope tagging was done as previously described (8). P1-mediated transduction was used to move mutations to different strains (9).

Microscopy- E. coli cells containing plasmids coding for Yfp-labeled proteins were grown at 30C in the presence of 10 µM IPTG (isopropyl ß-D-thiogalactoside) (10). Yfp-labeled cells were examined by fluorescence microscopy as previously described (10). Immunofluorescence experiments were done as previously described (11), except that the initial centrifugation steps were eliminated to avoid possible perturbation of protein localization. Cells were fixed in the growth medium at room temperature for one hour in the presence of 2% formaldehyde and 0.016% glutaraldehyde and then adsorbed on silane-coated cover slips. Monoclonal mouse anti-HA and polyclonal rabbit anti-Flag (Sigma) and Alexa fluor 488-conjugated goat anti-mouse and anti-rabbit antibodies (Molecular Probes) were used to detect HA and Flag-tagged RNase II. Images were not subjected to deconvolution. 200 to 300 cells were analyzed for each strain and the shown localization pattern was present in 90-95% of the cells.

Co-immunoprecipitation- Cells that co-express a chromosomally encoded RNase II-HA and a plasmid-encoded RNase II-Yfp derivative were grown at 30C to OD_{600} 0.4 and then the expression of the indicated Yfp-labeled proteins was induced for 4 hours by growth in the presence of 10 µM IPTG.

Cells that express chromosomally encoded RNase II-HA (AT67) or RNase II-Yfp (AT368) from the native P_{rnb} promoter were grown under the same condition except that IPTG was omitted. Equal amounts of AT67 and AT368 cells grown to the same cell density were combined in order to obtain protein extract containing both chromosomally expressed RNase II-HA and RNase II-Yfp proteins.

The cell pellets were washed twice with cold PBS buffer (10 mM Na_2HPO_4, 2 mM KH_2PO_4, 137 mM NaCl, 2.7 mM KCl), and then frozen at -70C. Protein extracts were prepared as previously described (12) except that: ***i.*** The cells were broken in a French pressure cell followed by three 20 seconds bursts of sonication at 4C; ***ii.*** EDTA-free protease inhibitor cocktail tablets were used in all solutions (Roche Diagnostics); ***iii.*** The ammonium sulfate pellet was resuspended in IP buffer (25 mM Tris pH 7.5, 150 mM NaCl, 1 mM DTT, 1 mM EDTA, 5% glycerol, 1% NP-40, and 1X protease inhibitor cocktail). Under these conditions 60 to 65 % of RNase II present in clarified cell lysates was recovered in the ammonium sulfate precipitates as shown by quantitative immunoblotting analysis. Protein concentrations were determined using a BCA assay kit (Pierce). Immunoprecipitations were carried out using protein A/G agarose beads according to manufacturer's instructions (Pierce) and polyclonal anti-HA or anti-Gfp antibodies (Santa Cruz Biotechnology), or rabbit IgG (Sigma). Beads were first incubated overnight at

4C in the presence of 1 mg protein extract in 0.5 ml IP buffer, and then washed three times with 0.5 ml IP buffer using spin columns. Retained proteins were eluted by incubating the beads for 5 min at room temperature in 50 µl elution buffer containing primary amine (pH 2.5) (Pierce) and then collected by centrifugation in tubes containing 3 µl 1M Tris buffer (pH 9.5) to neutralize the pH. Boiled samples were electrophoresed in 10% SDS mini-polyacrylamide gels and then electroblotted to nitrocellulose membrane in a Tris-glycine transfer buffer for 70 min with constant voltage of 100 V. Western blots were done using anti-HA and anti-Gfp (which binds Yfp protein) combined primary antibodies and alkaline phosphatase-conjugated anti-IgG secondary antibody (Sigma). When indicated, cell extracts were pre-incubated for 15 min at room temperature with 5 µg/ml of DNase-free bovine pancreatic RNase (Roche Diagnostics) prior to the overnight incubation with the beads (13). Complete degradation of RNA was obtained within 15 min of incubation at room temperature in IP buffer when RNase activity was tested on protein extracts supplemented with 200 µg/ml of yeast RNA (Sigma).

Membrane isolation- Cells were grown as described above for co-immunoprecipitation. Cells were broken in a French pressure cell and membranes fractions were prepared by a two-step sucrose gradient centrifugation as previously described (14). The SG0 fraction containing the total cell membranes was washed once with 10 ml cold HE buffer (10 mM Hepes pH 7.4, 5 mM EDTA) and then resuspended in the same buffer.

To quantitatively assess the RNase II membrane association, membrane and cytoplasm cellular fractions were prepared by ultracentrifugation of cell extracts as previously described (15,16).

Isolated membranes and cytoplasm were brought to the initial volume of the total protein extract and equal volumes from each fraction were loaded on SDS polyacrylamide gels and subjected to western blot analysis using anti-HA and anti-Gfp primary antibodies. Band intensities were proportional to the amount of protein applied to the gels and were quantified by densitometry using the ImageQuant program (Molecular Dynamics).

Immunoblotting analyses- To compare the expression levels of the Yfp-labeled RNase II derivatives, SDS total cell extracts were made using 1 ml culture from cells that were grown as indicated above for fluorescence microscopy. Cell samples were taken at 2.5, 4.5, 6.5 and 8.5 hours after addition of IPTG. The frozen cell pellets were resuspended in 10 mM Tris buffer pH 7.5 containing 1 mM EDTA and 4% SDS and then boiled for 5 min. Equal amounts of total protein extracts relative to the OD_{600} of the cultures were then separated on 10% polyacrylamide gels and electroblotted into nitrocellulose membranes. Band intensities were proportional to amounts of protein applied to gels. Anti-Gfp primary antibody (which binds Yfp protein) and alkaline phosphatase-conjugated anti-rabbit IgG secondary antibody were used to detect the Yfp-labeled RNase II derivatives.

RESULTS

Cellular organization of RNase II- Evidence that RNase II is organized within the cell and not uniformly distributed within the cytoplasm was shown by Yfp-labeling of plasmid-encoded RNase II and by tagging of the *rnb* chromosomal gene with Flag or HA epitopes, followed by fluorescence and immunofluorescence localization studies (Fig. 1A-D). RNase II-Yfp, RNase II-HA and RNase II-Flag proteins are functional proteins, as shown by their ability to restore viability to Δ*pnp* Δ*rnb* cells that lack PNPase and RNase II (below).

These studies showed that C-terminally-labeled RNase II-Yfp was localized within cellular structures that appeared to coil around the cell periphery, extending for considerable distances along the long axis of the cell (Fig. 1A). Immunofluorescence microscopy of cells expressing chromosomally encoded RNase II-Flag or RNase II-HA, using anti-Flag or anti-HA primary antibodies respectively, showed similar organized cellular structures (Fig. 1B-C). In contrast, N-terminally-labeled Yfp-RNase II showed a diffuse localization pattern presumably because Yfp obstructed binding of the protein to the membrane (see below) (Fig. 1D).

The cellular localization pattern of RNase II was not an artifact of Yfp-labeling (17) or cell fixation

since similar RNase II structures were observed both by fluorescence microscopy of live RNase II-Yfp cells and immunofluorescence microscopy of fixed cells that expressed RNase II-HA or RNase II-Flag. The organized cellular structures were not due to RNase II overexpression because similar localization patterns were obtained with cells that expressed higher than normal levels of plasmid-encoded RNase II-Yfp and cells that expressed chromosomally encoded RNase II-HA or RNase II-Flag under control of the native P_{rnb} promoter (Fig. 1A-C, 4F2).

Taken together the data show that RNase II exists within the cell as organized structures that appear associated with the cell periphery. These RNase II cellular structures resemble previously described long-range ordered structures of other *E. coli* proteins (11,18).

RNase II contains an amino-terminal amphipathic helix that acts as a membrane-binding anchor- We noted that the previously reported X-ray structure of RNase II shows an amino terminal helical domain that extends at roughly right angles from the body of the protein (Fig. 1I). The N-terminal helix (NTH) is not part of the adjacent OB-fold cold shock domain 1 and its function has not previously been elucidated (19,20). A helical wheel projection of the amino acid sequence of the NTH revealed an amphipathic character of the helical surfaces, with hydrophobic residues clustered on one face and polar residues on the other face (Fig. 1J). Because amphipathic helices act as membrane-binding anchors for other proteins (21-26), we asked whether the NTH of RNase II might play a role in binding the protein to the cytoplasmic membrane and/or in the formation of the organized cellular structures of the protein.

Evidence that RNase II is a membrane-associated protein and that the NTH domain is required for its membrane binding came from cell fractionation studies. The strain AT67/pFL4 co-expressed a chromosomally encoded RNase II-HA protein that showed an organized cellular pattern, and a plasmid-encoded RNase IIΔ^{19}-Yfp protein that lacked the NTH helix domain and showed a diffuse cytoplasmic distribution pattern (see below). The total membrane fraction isolated by sucrose gradient sedimentation (14) was analyzed by western blot using anti-Gfp (which interacts with Yfp) and anti-HA to identify RNase IIΔ^{19}-Yfp and RNase II-HA, respectively. As shown in Fig. 1K1, the membrane fraction contained the full-length HA-tagged RNase II but not the derivative that lacked the amphipathic helix domain. This shows that RNase II is a membrane-associated protein and that determinants in the NTH domain are required for the binding of the protein to the membrane.

To assess the RNase II membrane association, total membrane and cytoplasm fractions were isolated by ultracentrifugation (15,16) from the strain that co-expressed a chromosomally encoded RNase II-HA protein and a plasmid-encoded RNase IIΔ^{19}-Yfp protein, and then quantitatively analyzed by western blot using anti-Gfp and anti-HA antibodies. As illustrated in Fig. 1K2, the membrane fraction contained approximately 50% of the full-length HA-tagged RNase II but undetectable amounts of the derivative that lacked the amphipathic helix domain.

Parallel analyses of membrane and cytoplasmic fractions using antibodies against the known membrane-associated proteins MinD and MreB, which bind the membrane through an amphipathic helix, also showed approximately 50% of the proteins in the membrane fraction (Fig. 1K5-6). The presence of a portion of the protein in the cytoplasmic fraction may reflect partial dissociation of the peripheral membrane proteins during the process of cellular breakage and fractionation or dynamic membrane association of proteins within the cell.

Evidence that the NTH domain RNase II$^{(1\text{-}19)}$ is able to act as a transplantable membrane anchor that can direct normally cytoplasmic proteins to the membrane was obtained from localization studies of the Yfp-labeled NTH domain (RNase II$^{(1\text{-}19)}$-Yfp) and cell fractionation studies. Expression of the Yfp-labeled NTH domain in Δ*rnb* cells that lack endogenous RNase II showed a peripheral localization pattern characteristic of membrane-associated proteins (Fig. 1E). As expected, expression of free Yfp resulted in diffuse localization of Yfp throughout the cytoplasm (Fig. 1F).

Fractionation of cells that expressed RNase II$^{(1\text{-}19)}$-Yfp showed similar fractionation pattern as the full-length RNase II protein and the membrane

associated proteins MinD and MreB, that is, 51% of RNase II$^{(1-19)}$ was recovered with the membrane fraction (Fig. 1K3). This demonstrates that the NTH domain of RNase II can impart membrane-binding activity to the normally cytoplasmic Yfp protein. The NTH domain is therefore an autonomous membrane-binding domain.

The N-terminal helix is required for the RNase II cellular organization- To determine whether the membrane-binding domain of RNase II plays a role in the cellular organization of the protein, we carried out localization studies of plasmid-encoded Yfp-labeled RNase II derivatives in cells that lacked the endogenous *rnb* gene. Deletion of the first 19 residues of RNase II, including the entire amphipathic helix, led to loss of the organized structures observed with full-length RNase II. Instead, the RNase II$\mathbf{\Delta}^{19}$-Yfp was diffusely distributed within the cell, indicating a cytoplasmic localization (Fig. 1G). In contrast, deletion of the three residues that precede and lie outside of the amphipathic helix did not affect the ability of RNase II to assemble within the structures (Fig. 1H), indicating that these residues are not required for RNase II membrane binding and cellular organization.

Cellular fractionation studies further confirmed the subcellular localization of RNase II$\mathbf{\Delta}^{3}$ and RNase II$\mathbf{\Delta}^{19}$. RNase II$\mathbf{\Delta}^{19}$ was exclusively found in the cytoplasmic fraction (Fig. 1K2), whereas RNase II$\mathbf{\Delta}^{3}$ was associated with the membrane fraction, similar to full-length RNase II (Fig. 1K4). Taken together with the fact that RNase II$^{(1-19)}$-Yfp was peripherally localized with no evidence of organized structures (Fig. 1E), the data indicate that membrane binding of RNase II is required but is not sufficient for assembly of the organized membrane-associated cellular structures that are seen with full-length RNase II.

Role of amphipathicity of the RNase II N-terminal helix- We next used site-directed mutagenesis to address the role of the amphipathic character of the NTH in the membrane association and cellular organization of RNase II. To disrupt the amphipathicity of the helix within the full-length protein, four leucines of the hydrophobic face of the helix (Fig. 2A) were individually replaced by the polar amino acid aspartic acid. In all cases the Yfp-labeled L7D, L8D, L11D and L15D mutant proteins were diffusely distributed throughout the cytoplasm (Fig. 2B, F, J, N), indicating that the mutant proteins were incapable of binding the membrane and assembling into organized cellular structures. Diffuse localization patterns were also obtained when the mutations L7D, L8D, L11D or L15D were introduced into the RNase II$^{(1-19)}$-Yfp protein which contains the membrane-binding NTH domain in the absence of the rest of the RNase II protein (Fig. 2C, G, K, O), confirming that interference with the amphipathic nature of the NTH results in loss of membrane binding of its NTH domain.

In contrast, when the leucines were individually replaced by other hydrophobic amino acids (valine or isoleucine), the RNase II-Yfp L7V, L8V, L11V and L15I mutant proteins were organized into structures that were indistinguishable from the cellular structures formed by wild type RNase II-Yfp (Fig. 2D, H, L, P, Q). Similarly, replacement of polar amino acids with other polar amino acids in RNase II^{K12E}-Yfp and RNase II^{H16D}-Yfp did not affect the ability of the proteins to assemble into organized structures (Fig. 2E, I). Consistent with the observation that deletion of the residues that precede the amphipathic helix did not interfere with the normal cellular localization and organization of RNase II (Fig. 1H, K4), replacement of the second residue phenylalanine by lysine did not alter the cellular organization of RNase II (Fig. 2M). Quantitative western blot analysis showed similar cellular concentrations of all of the wild type and mutant proteins, indicating that the differences in localization pattern amongst the RNase II mutants and derivatives did not come from variations in cellular levels of the proteins (data not shown).

Consistent with the fluorescence localization studies of the RNase II mutants, cell fractionation experiments confirmed that the membrane association was completely abolished in L7D RNase II and RNase II$^{(1-19)}$ Yfp-labeled mutant proteins (Fig. 2R1-2) and was maintained similar to the wild type in L7V and K12E RNase II-Yfp mutants (Fig. 2R3-4).

Taken together, the data indicate that the amphipathic nature of the NTH is required for RNase II membrane association and for the organization of RNase II within the cell.

Specificity of RNase II amino-terminal membrane anchor- To investigate the sequence specificity of the NTH in directing the membrane-binding and cellular organization of RNase II, we replaced the RNase II NTH domain with the heterologous membrane-binding amphipathic helical domain of the MinD protein (MBD^{MinD}) (Fig. 3A). MBD^{MinD} was previously shown capable of acting as a membrane anchor when linked to Gfp or several cytoplasmic proteins (22,23,27). As opposed to the N-terminal membrane-binding domain of RNase II, MBD^{MinD} is located at the carboxyl end of the MinD protein. Replacing the RNase II NTH with MBD^{MinD} therefore reverses the relative orientation of the MBD^{MinD} amino acid sequence and its connectivity to MinD protein. Because of the possibility that the relative orientation of MBD^{MinD} to RNase II protein affects membrane binding, we studied the localization patterns of RNase II derivatives in which MBD^{MinD} or the reversed sequence of MBD^{MinD} (DBM^{MinD} Fig. 3A) replaced the RNase II NTH domain. As shown in Fig. 3B-C, **MBD^{MinD}**-RNase II**Δ^{19}**-Yfp and **DBM^{MinD}**-RNase II**Δ^{19}**-Yfp were localized into organized cellular structures independently of the orientation of the MinD membrane-binding domain. The cellular structures formed by the RNase II-MinD chimeras closely resembled the structures of the native RNase II protein (Fig. 1A-C, 3B-C). We conclude that the ability to support the membrane association and the assembly of RNase II into organized cellular structures is not restricted to the RNase II NTH membrane anchor.

We also asked whether the RNase II NTH domain could substitute for the MBD^{MinD} in supporting MinD membrane association and formation of the MinD cytoskeletal-like helical structures (18). As expected from previous studies, deletion of the last 10 residues of MinD, coding for the MBD^{MinD}, abrogated the membrane binding and the cytoskeletal-like organization of the MinD protein (Fig. 3E) (21,28). This was reversed by adding the RNase II NTH domain. Thus, the chimeric Yfp-$MinD^{(1-260)}$-**$NTH^{RNase\ II}$** was organized into cellular structures that coiled around the cell periphery and extended along the length of the cell (Fig. 3F). These structures were similar to the normal MinD cytoskeletal-like helical structures (18).

These experiments show that the RNase II and MinD membrane domains are interchangeable in supporting the membrane-binding and higher order cellular organization of the RNase II and MinD proteins.

To further investigate the specificity of the membrane anchor for the membrane association and cellular organization of RNase II, we replaced the RNase II NTH domain with the C-terminal amphipathic membrane-binding helix of the cell division protein FtsA (MBD^{FtsA}) (Fig. 3A). The MBD^{FtsA} was previously shown to act as an independent membrane anchor when appended to other proteins (23,29).

The chimeric MBD^{FtsA}-RNase IIΔ^{19}-Yfp protein was localized at the cell periphery but without any higher order organized structures of the protein (Fig. 3G). Thus, although the RNase II, MinD and FtsA membrane anchors were functionally interchangeable in recruiting RNase II to the membrane, only the RNase II and MinD MBDs were compatible with the assembly of RNase II into its characteristic organized cellular structures. The properties of these different membrane-binding domains are further discussed below.

Role of the membrane anchor in RNase II self-interaction- Why might membrane association be required for formation of the RNase II organized cellular arrays? Here we consider the possibility that membrane association of RNase II facilitates self-interaction of the protein that plays a role in the assembly of the RNase II long-range ordered cellular structures.

Evidence for RNase II self-association came from co-immunoprecipitation of differentially labeled RNase II proteins from protein extracts of cells that co-expressed chromosomally encoded RNase II-HA and plasmid-encoded RNase II-Yfp. Immunoprecipitates (IP) were obtained by using protein A/G beads coupled to anti-HA, anti-Gfp or IgG antibodies. The immunoprecipitates were then analyzed by western blots using anti-HA and anti-Gfp antibodies simultaneously. This showed the presence of both RNase II-HA and RNase II-Yfp in the IP fractions obtained with anti-HA beads (Fig. 4A1 right panel). Similarly, RNase II-HA and RNase II-Yfp were both present in the IP fractions obtained by immunoprecipitation with anti-Gfp beads (Fig. 4A2). In contrast, no RNase

II bands were detected in the IP fraction obtained with the IgG control beads (Fig. 4A1 left panel). The observed co-immunoprecipitation of RNase II-HA and RNase II-Yfp was consistent with RNase II-RNase II interactions within the cell extract.

Silver staining of the IP fraction obtained with anti-HA beads showed RNase II-HA and RNase II-Yfp as the only major bands in addition to the IgG bands (data not shown), consistent with direct RNase II-RNase II interactions. However, the possibility that one or more other proteins mediated the observed RNase II-RNase II interactions cannot be excluded.

Evidence that the RNase II interaction was not mediated by an RNA bridge (i.e., substrate-mediated association) came from immunoprecipitation of cell extracts that were pretreated with bovine pancreatic RNase. RNase II-HA and RNase II-Yfp bands were both present in the IP fractions obtained from RNase-treated extracts using anti-HA beads (Fig. 4A1), indicating that the degradation of RNA in the protein extracts did not alter the RNase II-RNase II interactions. This suggests that RNA does not play a role in the observed RNase II-RNase II interactions.

To determine whether the observed RNase II self-interaction was due to RNase II-Yfp overexpression, we compared parallel co-immunoprecipitations of differentially labeled RNase II proteins from protein extracts of cells that expressed RNase II-Yfp from a plasmid under the control of the P_{lac} promoter or from the chromosomal native P_{rnb} promoter. The cell extract that contains both of the chromosomally expressed RNase II-HA and RNase II-Yfp proteins was obtained by mixing equal amounts of AT67 and AT368 cells that expressed individual proteins respectively. These showed the presence of equivalent amounts of RNase II-Yfp in IP fractions obtained with anti-HA beads (Fig. 4F1) although the cellular level of the chromosomally expressed RNase II-Yfp was 10 fold lower compared to the level of plasmid-encoded protein (Fig. 4F2) as determined by quantitative western blots. The fact that similar extents of co-immunoprecipitation of RNase II-HA and RNase II-Yfp were obtained whether or not RNase II-Yfp was overexpressed shows that the RNase II interactions shown here were not artifacts of protein overexpression.

To determine whether the RNase II self-interaction required membrane association, we asked whether the interaction is dependent on the presence of the NTH domain. We performed the immunoprecipitation procedure on protein extracts from cells that co-expressed RNase II-HA, which contains the NTH and forms organized cellular structures (Fig. 1C), and RNase II$\mathbf{\Delta^{19}}$-Yfp, which fails to form organized structures and is located in the cytoplasm (Fig. 1G, K2). This showed that only a single band of the cognate RNase II-HA or RNase II$\mathbf{\Delta^{19}}$-Yfp was detected in the IP fractions obtained by immunoprecipitations with anti-HA or anti-Gfp beads, respectively (Fig. 4B right panels). We obtained similar results (Fig. 4C) from cells that co-expressed RNase II-HA and RNase II$^{\mathbf{L8D}}$-Yfp, which failed to form organized membrane-associated structures (Fig. 2F). Thus, the RNase II-RNase-II interaction was lost when one of the interacting partners lacked the NTH domain (RNase II$\mathbf{\Delta^{19}}$-Yfp) or the amphipathicity of its NTH domain was disrupted (RNase II$^{\mathbf{L8D}}$-Yfp). These results show that the RNase-II self-interaction requires the presence of functional membrane-binding domains on both interacting proteins, implying a requirement for RNase II membrane binding by both partners. This suggests that the interactions occur subsequent to entry of both partners into the membrane. Membrane anchors may also interact with small membrane vesicles that remained in cell extracts, or with lipid-detergent micelles within the amphiphilic media used for preparation of cell extracts and the immunoprecipitation experiments.

The data indicate that assembly of the RNase II organized cellular structures is associated with the ability of the protein to bind the membrane and to interact directly or indirectly with itself.

To ask whether the RNase II interaction is specific for the RNase II NTH domain, immunoprecipitation experiments were performed on extracts from cells that co-expressed RNase II-HA and a plasmid-encoded RNase II derivative in which the NTH domain was replaced by the membrane binding domain of MinD or FtsA. As shown in Fig. 4D, RNase II-HA and **MBD**$^{\mathbf{MinD}}$-RNase II$\mathbf{\Delta^{19}}$-Yfp were both found in the IP fractions obtained with anti-HA or anti-Gfp beads

but not detected in the IP fractions obtained with IgG control beads. The maintenance of interactions between RNase II derivatives that carry these different membrane anchors indicates that RNase II self-interaction does not occur via homotypic interactions between the membrane-binding anchors.

In contrast, no interaction was found when MBD^{FtsA} replaced the native membrane anchor of RNase II-Yfp. As shown in Fig. 4E, only a single protein band of RNase II-HA or $\mathbf{MBD^{FtsA}}$-RNase $\mathbf{II\Delta^{19}}$-Yfp was detected in the IP fractions obtained with anti-HA or anti-Gfp beads, respectively. The lack of interaction between RNase II and $\mathbf{MBD^{FtsA}}$-RNase $\mathbf{II\Delta^{19}}$ indicates that membrane binding of RNase II, although required, is not sufficient for the RNase II-RNase II interactions in cell extracts.

The $\mathbf{MBD^{FtsA}}$-RNase $\mathbf{II\Delta^{19}}$ derivative, in contrast to $\mathbf{MBD^{MinD}}$-RNase $\mathbf{II\Delta^{19}}$, failed to assemble into organized structures despite its membrane association (Fig. 3B, G). The FtsA MBD differs from the MBDs of RNase II and MinD in the higher hydrophobicity of its non-polar face. Thus, the hydrophobic moments of the RNase II, MinD and FtsA membrane binding domains were 0.373, 0.554 and 0.716, respectively (30). The FtsA MBD also contains more positively charged residues on its hydrophilic surface (Fig. 3A), increasing its amphipathic character. The possible role of these differences on the self-interaction properties of RNase II and the ability of the protein to assemble high order membrane-associated structures is discussed below.

Role of RNase II cellular organization in normal cell function- RNase II is essential for the viability of cells that lack PNPase, the other major exoribonuclease of the cell (3). This provided a means to evaluate the functional significance of the RNase II membrane association and cellular organization. We compared the ability of the plasmid-encoded RNase II derivatives to support normal growth in Δ*rnb* Δ*pnp* cells (FL4) that lacked the chromosomally encoded PNPase and RNase II proteins. Expression of RNase II or RNase II-Yfp in FL4/P_{lac}-*rnb* or FL4/P_{lac}-*rnb::yfp* cells in the presence of IPTG supported cell growth (Fig. 5A lanes 1-2 (+IPTG)). In contrast and consistent with the requirement of RNase II for cell viability in the absence of PNPase, repression of RNase II or RNase II-Yfp expression by growth in the presence of glucose blocked cell growth (Fig. 5A lanes 1-2 (+glucose)). Disruptions of the amphipathicity of the RNase II NTH that lead to cytoplasmic localization of the protein (RNase II^{L7D}, RNase II^{L8D}) were associated with a significant decrease in growth rate of Δ*rnb* Δ*pnp* cells (Fig. 5A lanes 2-4; Fig. 5B). In contrast, conservative mutations of the NTH of RNase II that maintained the normal cellular organization pattern of the wild type protein (RNase II^{L7V}, RNase II^{L8V}) supported normal growth in Δ*rnb* Δ*pnp* cells (Fig. 5A lanes 5-6; Fig. 5B). This suggested that the ability of RNase II to associate with the membrane and/or to assemble into higher order organized cellular structures is required for the maintenance of normal growth in cells that lack PNPase.

Evidence that the ability of RNase II-Yfp to maintain viability of Δ*pnp* Δ*rnb* cells was not due to overexpression of the plasmid-encoded RNase II-Yfp came from comparison of growth rates of Δ*pnp* Δ*rnb* cells whose *rnb* gene was replaced by a plasmid-encoded *rnb::yfp* under P_{lac} control (FL4/pFL3) and Δ*pnp* cells whose *rnb* gene was replaced by a chromosomally encoded *rnb::yfp* under the native P_{rnb} promoter (AT372). As shown in Fig. 5B, both strains grew at similar growth rates independently of the expression levels of RNase II-Yfp (Fig. 4F2). Thus, the observed complementation of Δ*pnp* Δ*rnb* cells was not due to overexpression of RNase II-Yfp.

The chimeric RNase II protein in which the MBD^{MinD} replaced the RNase II NTH domain, which exhibited the normal organization pattern of RNase II, behaved similarly to wild type RNase II in its ability to restore normal growth to the Δ*rnb* Δ*pnp* strain (Fig. 5A lane 7). In contrast the $\mathbf{MBD^{FtsA}}$-RNase $\mathbf{II\Delta^{19}}$-Yfp protein that shows peripheral localization but fails to assemble the normal organized cellular patterns failed to restore growth in the Δ*rnb* Δ*pnp* cells. This was shown by the inability to produce colonies in the presence of a wide range of concentrations of IPTG after the attempted introduction of a Δ*pnp-cat* mutation into the Δ*rnb*/P_{lac}- $\boldsymbol{MBD^{FtsA}}$*::rnb*$\boldsymbol{\Delta^{19}}$*::yfp* cells by P1 transduction or by λ Red-mediated gene replacement (7,9). This was done under conditions

that gave a large number of Δ*pnp* colonies in parallel experiments using Δ*rnb/P*$_{lac}$*-rnb* or Δ*rnb/P*$_{lac}$*-rnb::yfp* recipient cells. This indicates that RNase II membrane association alone is insufficient to restore normal cellular function.
Taken together, the data suggest that the RNase II higher order cellular organization is required for normal cell growth in Δ*pnp* cells.

DISCUSSION

Localization studies of RNase II, the major exoribonuclease of *E. coli*, using fully functional Yfp-labeled and epitope-tagged RNase II proteins, showed that the protein is not diffuse within the cytoplasm but rather organized as long-range cellular structures that appear to coil around the cell periphery. The present work also shows that an N-terminal amphipathic helix (NTH) of RNase II acts as a membrane-binding anchor that is required for the assembly of RNase II into organized cellular structures. Assembly of the RNase II cellular structures is dependent on the ability of the protein to bind the cytoplasmic membrane via the amphipathic anchor, as shown by the observation that deletion of the RNase II NTH domain or perturbation of its amphipathicity abrogated membrane association and assembly of the organized cellular structures.

It is also clear that assembly of the RNase II cellular structures requires determinants outside of the membrane anchor. This was shown by the inability of the NTH domain of NTH-Yfp to form organized cellular structures in the absence of other RNase II domains despite the fact that the NTH domain alone was capable of recruiting Yfp to the membrane.

Proteins of the *E. coli* MreBCD and MinCDE cytoskeletal-like systems also rely on amphipathic helix membrane anchors for their cellular organization. The amino-terminal helix of MreB and carboxy-terminal helix of MinD respectively are required for assembly of MreB cellular structures (24) which are essential for cell shape maintenance, or for formation of the helically organized MinD structures that are required for proper placement of the division site at midcell (31). In these systems, the membrane anchor is located on the surface of the membrane, oriented parallel to the bilayer surface. The membrane association is mediated by interactions of lipid acyl chains of the bilayer with nonpolar amino acids chains that extend from one face of the amphipathic helix into the bilayer structure (24,28,32). A similar mechanism for membrane binding is likely for the NTH domain of RNase II as this successfully replaced the MBD$^{\mathbf{MinD}}$ in supporting membrane association and assembly of the MinD cytoskeletal-like structures.

Assembly of the organized RNase II cellular structures is also dependent on the ability of the protein to interact directly or indirectly with itself, as shown by co-immunoprecipitation studies. The RNase II interactions require the presence of a membrane-binding domain on both interacting RNase II partners, implying that membrane association is required for the RNase II self-interactions. It is possible that these interactions may also involve interactions between adjacent membrane anchor domains. However, the X-ray structure of RNase II shows that the NTH domains of adjacent molecules are oriented away from each other and from the subunit interfaces of the protein (20), arguing against the likelihood that direct interaction between NTH domains mediates the observed RNase II self-interaction.

The results are compatible with a model in which membrane binding of RNase II is associated with a change in conformation that leads to RNase II self-association that plays a role in its subsequent assembly into membrane-associated organized cellular structures. The RNase II self-association shown by co-immunoprecipitation from cell extracts could reflect either direct RNase II-RNase II interactions or the association of RNase II molecules via interactions with other components of the RNA processing and degradation machinery.

The RNase II cellular structures were maintained when the unrelated MinD MBD replaced the RNase II NTH membrane anchor. In contrast, assembly of the RNase II organized structures was lost when the FtsA MBD directed the protein to the membrane. The FtsA MBD differs from the MBDs of RNase II and MinD by the higher amphipathicity of its helix. MBD$^{\mathbf{FtsA}}$ is therefore likely to bind more tightly to the membrane surface. This could affect the conformation or orientation of the membrane-associated protein, thereby hindering RNase II

interactions that are required for assembly of its characteristic organized cellular structures.

It is of interest that many of the proteins involved in RNA processing and degradation also contain potential membrane-binding domains. Thus, the endoribonuclease RNaseE contains an internal amphipathic helix that can act as a membrane anchor to associate the protein with lipid vesicles (33); PAP I contains a potential membrane-binding domain within its first 24 amino acids (34,35); Hfq is localized in close proximity to the cytoplasmic membrane in electron microscopic studies (36); and the endoribonucleases RNase III and RNase P were found in inner membrane fractions in cell fractionation studies (37). Whether other components of the RNA processing and degradation are also membrane associated and whether membrane-association of these proteins is required for their proper cellular organization and function, as is the case for RNase II, remains to be determined.

What might be the biological role of the membrane association and cellular organization of RNase II? Mutations of the NTH that interfered with formation of the RNase II organized structures were associated with a significant defect in the growth of cells that lack PNPase and RNase II. This suggests that the cellular organization of RNase II might be required for the enzyme to carry out essential cellular functions. The growth defect could come from loss of the cellular organization of RNase II or/and from a direct effect of the NTH mutations on the intrinsic catalytic activity of the enzyme. Arguing against the second possibility are previous studies showing that RNase II derivatives with deletions of the first 38 or 84 residues of the protein, which remove the NTH membrane binding domain, were as efficient as full-length RNase II in degrading RNA substrates *in vitro* (38). Nonetheless, it remains to be directly determined whether the mutations described here, which are restricted to individual residues within the NTH domain, interfere with the exoribonuclease activity of the isolated proteins.

There are several possible biological roles for the assembly of RNase II into its characteristic organized membrane-associated structures. ***i***. The membrane association may play a regulatory role by modulating the enzymatic activity of the protein. ***ii***. The cytoplasmic membrane may act as a matrix to facilitate interactions of RNase II with itself or with other components of the RNA processing and degradation machinery by increasing the local concentration, due to confinement to the two-dimensional membrane milieu, or by altering the conformation of the protein. ***iii***. The higher order organization of the protein might sequester RNase II and other components of the cellular RNA processing and degradation, such as the RNA degradosome, within a common compartment. This could serve as a mechanism to bring in close proximity protein partners that act cooperatively on their RNA substrates, and/or keep the proteins away from the cytoplasm to prevent premature degradation of RNA substrates. These possibilities are not mutually exclusive. Further work will be needed to define the nature of the apparent higher order RNase II structures in the cell and the role of the membrane association and cellular organization of the protein in the essential RNA degradation and processing functions of the bacterial cell.

REFERENCES

1. Nossal, N. G., and Singer, M. F. (1968) *J. Biol. Chem.* **243**(5), 913-922
2. Deutscher, M. P., and Reuven, N. B. (1991) *Proc. Natl. Acad. Sci. U S A* **88**(8), 3277-3280
3. Donovan, W. P., and Kushner, S. R. (1986) *Proc. Natl. Acad. Sci. U S A* **83**(1), 120-124
4. Li, Z., Pandit, S., and Deutscher, M. P. (1998) *Proc. Natl. Acad. Sci. U S A* **95**(6), 2856-2861
5. Li, Z., and Deutscher, M. P. (1996) *Cell* **86**(3), 503-512
6. Maniatis, T., Fritsch, E. F., and Sambrook, J. (1982) *Molecular Cloning: A Laboratory Manual.*, Cold Spring Harbor Laboratory, Cold Spring Harbor, New York
7. Datsenko, K. A., and Wanner, B. L. (2000) *Proc. Natl. Acad. Sci. U S A* **97**(12), 6640-6645
8. Uzzau, S., Figueroa-Bossi, N., Rubino, S., and Bossi, L. (2001) *Proc. Natl. Acad. Sci. U S A* **98**(26), 15264-15269

9. Miller, J. H. (1992) *A short course on bacterial genetics*, Cold Spring Harbor Laboratory Press, Cold Spring Harbor, N.Y.
10. Shih, Y. L., Fu, X., King, G. F., Le, T., and Rothfield, L. (2002) *Embo J.* **21**(13), 3347-3357
11. Taghbalout, A., and Rothfield, L. (2007) *Proc. Natl. Acad. Sci. U S A* **104**(5), 1667-1672
12. Carpousis, A. J., Van Houwe, G., Ehretsmann, C., and Krisch, H. M. (1994) *Cell* **76**(5), 889-900
13. Carpousis, A. J., Khemici, V., Ait-Bara, S., and Poljak, L. (2008) *Methods Enzymol.* **447**, 65-82
14. Ishidate, K., Creeger, E. S., Zrike, J., Deb, S., Glauner, B., MacAlister, T. J., and Rothfield, L. I. (1986) *J. Biol. Chem.* **261**(1), 428-443
15. Murashko, O. N., Kaberdin, V. R., and Lin-Chao, S. (2012) *Proc. Natl. Acad. Sci. U S A* **109**(18), 7019-7024
16. Fujiki, Y., Hubbard, A. L., Fowler, S., and Lazarow, P. B. (1982) *J. Cell Biol.* **93**(1), 97-102
17. Swulius, M. T., and Jensen, G. J. (2012) *J. bacteriol.* **194**(23), 6382-6386
18. Shih, Y. L., Le, T., and Rothfield, L. (2003) *Proc. Natl. Acad. Sci. U S A* **100**(13), 7865-7870
19. Frazao, C., McVey, C. E., Amblar, M., Barbas, A., Vonrhein, C., Arraiano, C. M., and Carrondo, M. A. (2006) *Nature* **443**(7107), 110-114
20. Zuo, Y., Vincent, H. A., Zhang, J., Wang, Y., Deutscher, M. P., and Malhotra, A. (2006) *Mol. Cell* **24**(1), 149-156
21. Hu, Z., and Lutkenhaus, J. (2003) *Mol. Microbiol.* **47**(2), 345-355
22. Szeto, T. H., Rowland, S. L., Habrukowich, C. L., and King, G. F. (2003) *J. Biol. Chem.* **278**(41), 40050-40056
23. Pichoff, S., and Lutkenhaus, J. (2005) *Mol. Microbiol.* **55**(6), 1722-1734
24. Salje, J., van den Ent, F., de Boer, P., and Lowe, J. (2011) *Mol. Cell* **43**(3), 478-487
25. Jackson, M. E., and Pratt, J. M. (1988) *Mol. Microbiol.* **2**(5), 563-568
26. Shih, Y. L., Huang, K. F., Lai, H. M., Liao, J. H., Lee, C. S., Chang, C. M., Mak, H. M., Hsieh, C. W., and Lin, C. C. (2011) *PloS one* **6**(6), e21425
27. Taghbalout, A., Ma, L., and Rothfield, L. (2006) *J. Bacteriol.* **188**(8), 2993-3001
28. Szeto, T. H., Rowland, S. L., Rothfield, L. I., and King, G. F. (2002) *Proc. Natl. Acad. Sci. U S A* **99**(24), 15693-15698
29. Osawa, M., Anderson, D. E., and Erickson, H. P. (2008) *Science (New York, N.Y* **320**(5877), 792-794
30. Gautier, R., Douguet, D., Antonny, B., and Drin, G. (2008) *Bioinformatics* **24**(18), 2101-2102
31. Rothfield, L., Taghbalout, A., and Shih, Y. L. (2005) *Nat. Rev. Microbiol.* **3**(12), 959-968
32. Hu, Z., Gogol, E. P., and Lutkenhaus, J. (2002) *Proc. Natl. Acad. Sci. U S A* **99**(10), 6761-6766
33. Khemici, V., Poljak, L., Luisi, B. F., and Carpousis, A. J. (2008) *Mol. Microbiol.* **70**(4), 799-813
34. Jasiecki, J., and Wegrzyn, G. (2005) *Biochem. Biophys. Res. Commun.* **329**(2), 598-602
35. Carabetta, V. J., Mohanty, B. K., Kushner, S. R., and Silhavy, T. J. (2009) *J. Bacteriol.* **191**(22), 6812-6821
36. Diestra, E., Cayrol, B., Arluison, V., and Risco, C. (2009) *PloS one* **4**(12), e8301
37. Miczak, A., Srivastava, R. A., and Apirion, D. (1991) *Mol. Microbiol.* **5**(7), 1801-1810
38. Amblar, M., Barbas, A., Fialho, A. M., and Arraiano, C. M. (2006) *J. Mol. Biol.* **360**(5), 921-933
39. Delano, W. L. (2005) The PyMOL Molecular Graphics System, Version 0.98. In., DeLano Scientific LLC, South San Fransisco
40. de Boer, P. A., Crossley, R. E., and Rothfield, L. I. (1989) *Cell* **56**(4), 641-649
41. Covarrubias, L., Cervantes, L., Covarrubias, A., Soberon, X., Vichido, I., Blanco, A., Kupersztoch-Portnoy, Y. M., and Bolivar, F. (1981) *Gene* **13**(1), 25-35
42. Cherepanov, P. P., and Wackernagel, W. (1995) *Gene* **158**(1), 9-14
43. Rowland, S. L., Fu, X., Sayed, M. A., Zhang, Y., Cook, W. R., and Rothfield, L. I. (2000) *J. Bacteriol.* **182**(3), 613-619
44. Morita, T., Kawamoto, H., Mizota, T., Inada, T., and Aiba, H. (2004) *Mol. Microbiol.* **54**(4), 1063-1075

Acknowledgements- We thank L. Rothfield and M. Osborn for critical reading of the manuscript.

FOOTNOTES

*This work was supported by NIH grant R37 GM060632.

[1]To whom correspondence should be addressed: Aziz Taghbalout, Department of Molecular, Microbial, and Structural Biology, University of Connecticut Health Center, 263 Farmington Avenue, Farmington, CT, 06032, USA. Tel.: (860) 679-4208; Fax: (860) 679-1239, Email: taghbalout@neuron.uchc.edu

[2]The abbreviations used are: DBM, reversed orientation of the membrane-binding domain; FT, Flow through; IP, Immunoprecipitate; IPTG, Isopropyl ß-D-thiogalactoside; MBD, Membrane-binding domain; NP-40, Nonidet P-40; NTH, N-terminal helix; OB, Oligonucleotide/oligosaccharide binding; OD, Optical density; PE, Protein extract.

[3]Research Collaboratory for Structural Bioinformatics Protein Databank = PDB # 2ID0

FIGURE LEGENDS

Figure 1- Role of the amino terminal amphipathic helix in membrane-binding and cellular organization of RNase II.

(A-H) Micrographs of Yfp fluorescence of the plasmid-encoded RNase II proteins in the indicated strains and immunofluorescence of the chromosomally encoded Flag or HA-tagged RNase II are shown. **Panel A**- FL1/pFL3 cells *(Δrnb/ P_{lac}-rnb::yfp)*; **panel B**- AT68 (*rnb::Flag*); **panel C**- AT67 (*rnb::HA*); **panel D**- FL1/pFL1 *(Δrnb/ P_{lac}-yfp::rnb)*; **panel E**- FL1/pFL13 *(Δrnb/ P_{lac}-rnb$^{(1-19)}$::yfp)*; **panel F**- MC1000/pAT80 *(wt/ P_{lac}-yfp)*; **panel G**- FL1/pFL4 *(Δrnb/ P_{lac}-rnbΔ^{19}::yfp)*; **panel H**- FL1/pFL30 *(Δrnb/ P_{lac}-rnbΔ$^{(2-4)}$::yfp)*. Scale bar = 1 µm. 200 to 300 cells were analyzed for each strain and the shown localization pattern was present in 90-95% of the cells (Experimental Procedures).

(I)- X-ray structure of RNase II showing the amino-terminal helix (red), the nucleic acid binding OB fold domains (blue) and the ribonuclease catalytic domain (grey). Image generated according to (19,20), using PyMOL molecular graphics system (39) and RNase II protein (protein data bank accession number 2ID0)[3]. **(J)**- Helical wheel projection of the RNase II amino terminal helix using the HeliQuest program (30). Nonpolar (yellow), polar noncharged (black) and polar charged residues (blue) are shown. The amino-acid sequence of the NTH domain with its secondary structure is shown.

(K) Western blot analysis of membrane fraction isolated by sucrose gradient centrifugation (14) (panel 1), and membrane and cytoplasm fractions isolated by ultracentrifugation (15,16) (panels 2-6) using monoclonal antibodies anti-HA and anti-Gfp (panels 1-4) or purified polyclonal antibodies anti-MinD (panel 5) or anti-MreB (panel 6) and the indicated cellular fractions from cells that co-expressed chromosomally encoded HA-tagged RNase II and plasmid-encoded Yfp-labeled RNase II mutants is shown. **Panels 1-2, 5-6**- AT67/pFL4 cells (*rnb::HA/ P_{lac}-rnbΔ^{19}::yfp*); **panel 3**- AT67/pFL13 cells (*rnb::HA/ P_{lac}-rnb$^{(1-19)}$::yfp*); **panel 4**- AT67/pFL30 cells (*rnb::HA/ P_{lac}-rnbΔ$^{(2-4)}$::yfp*). Isolated cellular fractions were brought to the same volume as the protein extract and then equal volumes from total protein extract (lanes 1-3), membranes (lanes 4-6) and cytoplasm (lanes 7-9) were loaded as indicated. **Panel 1**- 2 µl, 4 µl or 8 µl from each sample were loaded in lanes 1 and 4, lanes 2 and 5, or lanes 3 and 6 respectively; **panels 2-6**- 8 µl, 4 µl or 2 µl from each sample were loaded in lanes 1, 4 and 7, lanes 2, 5 and 8, or lanes 3, 6 and 9 respectively. Arrows indicate positions of protein bands of Yfp-labeled RNase II mutants (green), HA-tagged RNase II (white) and MinD (black), arrowhead indicates MreB bands and *rnb*** indicates *rnb* mutants.

Figure 2- Role of the amphipathic character of RNase II NTH.

(A) Helical wheel projection and amino acid sequence of the RNase II amphipathic helix is shown. Nonpolar (white), polar (black) and polar charged residues (grey) are shown. The mutated residues are shaded in grey in the amino-acid sequence and are marked by stars in the shown helical wheel projection.

(B-Q) Fluorescence micrographs of the indicated Yfp-labeled RNase II proteins are shown. Scale bar = 1 µm. **Panel B**- FL1/pFL7 cells (*Δrnb/ P_{lac}-rnb^{L7D}::yfp*); **panel C**- FL1/pFL16 cells (*Δrnb/ P_{lac}-rnb$^{(1-19)L7D}$::yfp*); **panel D**- FL1/pFL21 cells (*Δrnb/ P_{lac}-rnb^{L7V}::yfp*); **panel E**- FL1/pFL26 cells (*Δrnb/ P_{lac}-rnb^{K12E}::yfp*); **panel F**- FL1/pFL8 cells (*Δrnb/ P_{lac}-rnb^{L8D}::yfp*); **panel G**- FL1/pFL17 cells (*Δrnb/ P_{lac}-rnb$^{(1-19)L8D}$::yfp*); **panel H**- FL1/pFL22 cells (*Δrnb/ P_{lac}-rnb^{L8V}::yfp*); **panel I**- FL1/pFL25 cells (*Δrnb/ P_{lac}-rnb^{H16D}::yfp*); **panel J**- FL1/pFL9 cells (*Δrnb/ P_{lac}-rnb^{L11D}::yfp*); **panel K**- FL1/pFL18 cells (*Δrnb/ P_{lac}-rnb$^{(1-19)L11D}$::yfp*); **panel L**- FL1/pFL23 cells (*Δrnb/ P_{lac}-rnb^{L11V}::yfp*); **panel M**- FL1/pFL31 cells (*Δrnb/ P_{lac}-rnb^{F2K}::yfp*); **panel N**- FL1/pFL10 cells (*Δrnb/ P_{lac}-rnb^{L15D}::yfp*); **panel O**- FL1/pFL20 cells (*Δrnb/ P_{lac}-rnb$^{(1-19)L15D}$::yfp*); **panel P**- FL1/pFL24 cells (*Δrnb/ P_{lac}-rnb^{L15I}::yfp*); **panel Q**- FL1/pFL3 cells (*Δrnb/ P_{lac}-rnb::yfp*).

(R) Western blot analysis using monoclonal antibodies anti-HA and anti-Gfp (panels 1-4) and indicated cellular fractions that were isolated by ultracentrifugation (15,16) from cells that co-expressed chromosomally encoded HA-tagged RNase II and plasmid-encoded Yfp-labeled RNase II mutant is shown. **Panel 1**- AT67/pFL7 cells (*rnb::HA/ P_{lac}-rnb^{L7D}::yfp*); **panel 2**- AT67/pFL16 cells (*rnb::HA/P_{lac}-rnb$^{(1-19)L7D}$::yfp*); **panel 3**- AT67/pFL21 cells (*rnb::HA/ P_{lac}-rnb^{L7V}::yfp*); **panel 4**- AT67/pFL26 cells (*rnb::HA/ P_{lac}-rnb^{K12E}::yfp*). Samples were applied to gels as indicated in legend to Fig. 1K2-6. Arrows and arrowheads indicate positions of protein bands of Yfp-labeled RNase II mutant and HA-tagged RNase II respectively, and *rnb*** indicates *rnb* mutants.

Figure 3- The amino-terminal helix of RNase II is a transplantable membrane-binding domain.

(A)- NTH domain of RNase II and the membrane-binding domains (MBD) of MinD and FtsA are shown as helical wheel projections of their corresponding amphipathic terminal helices. MinD and FtsA helices are drawn according to previous reports (21,23). MinD DMB is the reversed orientation of the amino acid sequence of MinD MBD. N and C indicate the amino and carboxyl termini of the helices.

(B-G)- Fluorescence micrographs of the Yfp-labeled proteins from the indicated strains are shown. **Panel B**- FL1/pFL11 (*Δrnb/ P_{lac}-**MBD**^{minD}::rnbΔ^{19}::yfp*); **panel C**- FL1/pFL12 (*Δrnb/ P_{lac}-**DBM**^{minD}::rnbΔ^{19}::yfp*); **panel D**- FL1/pFL4 (*Δrnb/ P_{lac}-rnbΔ^{19}::yfp*); **panel E**- RC1/pAT5 (*ΔminCDE/ P_{lac}-yfp::minDΔ$^{(261-270)}$*); **panel F**- RC1/pFL15 (*ΔminCDE/ P_{lac}-yfp::minDΔ$^{(261-270)}$::rnb$^{(1-19)}$*); **panel G**- FL1/pFL32 (*Δrnb/ P_{lac}-**MBD**^{ftsA}::rnbΔ^{19}::yfp*). Δ*min* cells grew as mixed populations of long and normal sized cells as well as minicells (40). Scale bar = 1 µm.

Figure 4- RNase II self-association.

Co-immunoprecipitation with anti-HA (A1-E1 (right side) and F1), anti-Gfp (A2-E2 (right side)) or IgG (A-E (left side)) beads of protein extract from cells that expressed the indicated RNase II derivatives. Protein extracts (PE (3 µg)) and immunoprecipitation fractions, flow through (FT) and immunoprecipitate (IP), obtained with the indicated IgG, anti-HA or anti-Gfp beads were subjected to western blots using combined anti-HA and anti-Gfp polyclonal (panels A-E) or monoclonal (panel F1) antibodies. Drawings depict beads used to obtain the fractions analyzed in the adjacent gel. **(A)** AT67/pFL3 (*rnb::HA/P_{lac}-rnb::yfp*); **(B)** AT67/pFL4 (*rnb::HA/ P_{lac}-rnbΔ^{19}::yfp*); **(C)** AT67/pFL8 (*rnb::HA/ P_{lac}-rnb^{L8D}::yfp*); **(D)** AT67/pFL11 (*rnb::HA/ P_{lac}-**MBD**^{minD}::rnbΔ^{19}::yfp*); **(E)** AT67/pFL32 (*rnb::HA/ P_{lac}-**MBD**^{ftsA}::rnbΔ^{19}::yfp*); **(F)** AT67/pFL3 (*rnb::HA/ P_{lac}-rnb::yfp*) (left), AT67 (*rnb::HA*) + AT368 (*rnb::yfp*) (right). To determine the extent of overexpression of the plasmid-encoded RNase II-Yfp same (1X) or three-time (3X) protein amounts of cell extracts from AT67/pFL3 and AT67+AT368 cells were applied to gels and immunoblotted with monoclonal (F2 top panels) or polyclonal (F2 bottom panels) antibodies as indicated. When indicated, protein extracts were pretreated with RNase from bovine pancreas as described in Experimental Procedures (panels A1, D2). Empty arrows show the positions of Yfp-tagged RNase II derivatives and black arrows show the positions of HA-tagged RNase II bands.

Figure 5- Effect of the RNase II mutations on cell growth.

Complementation assays to compare the ability of the RNase II derivatives to rescue FL4 cells (Δ*rnb* Δ*pnp*). (**A**) Mid-log phase cultures of FL4 strains harboring the indicated plasmids were adjusted to the same optical density (OD_{600}), serially diluted (10^{-1}-10^{-5}) and then 1 µl of each culture was spotted on agar plates containing 50 µM IPTG or 0.4 % glucose. Similar results were obtained when the plates contained 150 µM IPTG, or when *rnb-HA* and *rnb-Flag* replaced the chromosomal copy of *rnb* gene in FL2 (Δ*pnp rnb::HA*) and FL3 (Δ*pnp rnb::Flag*) cells respectively (data not shown). (**B**) Growth curves of FL4 and AT372 cells expressing under P_{lac} control the indicated plasmid-encoded RNase II-Yfp derivatives in the presence of 10 µM IPTG or RNase II-Yfp under the control of P_{rnb} chromosomal promoter are respectively shown. The presence of higher IPTG concentrations (50 and 100 µM) gave similar growth. **White circles**- AT372 (Δ*pnp rnb::yfp*); **black circles**- FL4/pFL3 (Δ*rnb* Δ*pnp/* P_{lac}*-rnb::yfp*); **white squares**- FL4/pFL22 (Δ*rnb* Δ*pnp/* P_{lac}*-rnb*^{L8V}*::yfp*); **black squares**- FL4/pFL21 (Δ*rnb* Δ*pnp/* P_{lac}*-rnb*^{L7V}*::yfp*); **stars**- FL4/pFL7 (Δ*rnb* Δ*pnp/* P_{lac}*-rnb*^{L7D}*::yfp*); **black triangles**- FL4/pFL8 (Δ*rnb* Δ*pnp/* P_{lac}*-rnb*^{L8D}*::yfp*).

Table 1- Plasmids and strains

Plasmids	Relevant Genotype or Description	Reference or source
pMLB1113[a]	Low copy number vector (18 per cell)	(40,41)
pAT5	P_{lac}-*yfp::minD*$\Delta^{(261-270)}$	(27)
pAT80	P_{lac}-*yfp*	This study
pFL1	P_{lac}-*yfp::rnb*	This study
pFL3	P_{lac}-*rnb::yfp*	This study
pFL4	P_{lac}-*rnb*$\Delta^{(1-19)}$*::yfp*	This study
pFL6	P_{lac}-*rnb*	This study
pFL7	P_{lac}-*rnb*^{L7D}*::yfp*	This study
pFL8	P_{lac}-*rnb*^{L8D}*::yfp*	This study
pFL9	P_{lac}-*rnb*^{L11D}*::yfp*	This study
pFL10	P_{lac}-*rnb*^{L15D}*::yfp*	This study
pFL11	P_{lac}-*MBD*^{minD}*::rnb*$\Delta^{(1-19)}$*::yfp* (MinD$^{(255-270)}$)	This study
pFL12	P_{lac}-*DBM*^{minD}*::rnb*$\Delta^{(1-19)}$*::yfp* (MinD$^{(270-255)}$)	This study
pFL13	P_{lac}-*rnb*$^{(1-19)}$*::yfp*	This study
pFL15	P_{lac}-*yfp::minD*$\Delta^{(261-270)}$*::rnb*$^{(1-19)}$	This study
pFL16	P_{lac}-*rnb*$^{(1-19)L7D}$*::yfp*	This study
pFL17	P_{lac}-*rnb*$^{(1-19)L8D}$*::yfp*	This study
pFL18	P_{lac}-*rnb*$^{(1-19)L11D}$*::yfp*	This study
pFL20	P_{lac}-*rnb*$^{(1-19)L15D}$*::yfp*	This study
pFL21	P_{lac}-*rnb*^{L7V}*::yfp*	This study
pFL22	P_{lac}-*rnb*^{L8V}*::yfp*	This study
pFL23	P_{lac}-*rnb*^{L11V}*::yfp*	This study
pFL24	P_{lac}-*rnb*^{L15I}*::yfp*	This study
pFL25	P_{lac}-*rnb*^{H16D}*::yfp*	This study
pFL26	P_{lac}-*rnb*^{K12E}*::yfp*)	This study
pFL30	P_{lac}-*rnb*$\Delta^{(2-4)}$*::yfp*	This study
pFL31	P_{lac}-*rnb*^{F2K}*::yfp*	This study
pFL32	P_{lac}-*MBD*^{ftsA}*::rnb*$\Delta^{(1-19)}$*::yfp* (FtsA$^{(406-420)}$)	This study
pKD4	*kan marker for gene deletion constructs*	(7)
pKD46	*Red recombinase expression plasmid*	(7)
pCP20	*FLP expression plasmid*	(42)
pSU312	*Flag-kan*	(8)
pSU315	*HA-kan*	(8)
Strains	**Relevant Genotype or Description**	**Reference or source**
MC1000	*F- araD139 Δ(araABC-leu)7679 galU galK Δ(lac)X74 rpsL thi*	(40)
RC1	*MC1000* Δ*minCDE*-kan	(43)
AT67	*MC1000 rnb::HA-kan*	This study
AT68	*MC1000 rnb::Flag-kan*	This study
AT368	*MC1000 rnb::yfp-kan*	This study
AT372	*MC1000* Δ*pnp-cat rnb::yfp-kan*	This study
FL1	*MC1000* Δ*rnb-kan*	This study
FL2	*AT67* Δ*pnp-cat*	This study
FL3	*AT68* Δ*pnp-cat*	This study
FL4[b]	*MC1000* Δ*rnb-kan* Δ*pnp-cat*	This study
TM388	Δ*pnp-cat*	(44)

[a/] Plasmids pAT and pFL are made in pMLB1113 vector.
[b/] Strain not viable unless complemented.

To allow selection during construction of HA, Flag and *yfp* chromosomal fusions and deletion strains, a kanamycin-resistance cassette was inserted by linear DNA recombination (Experimental Procedures).

Figure 1

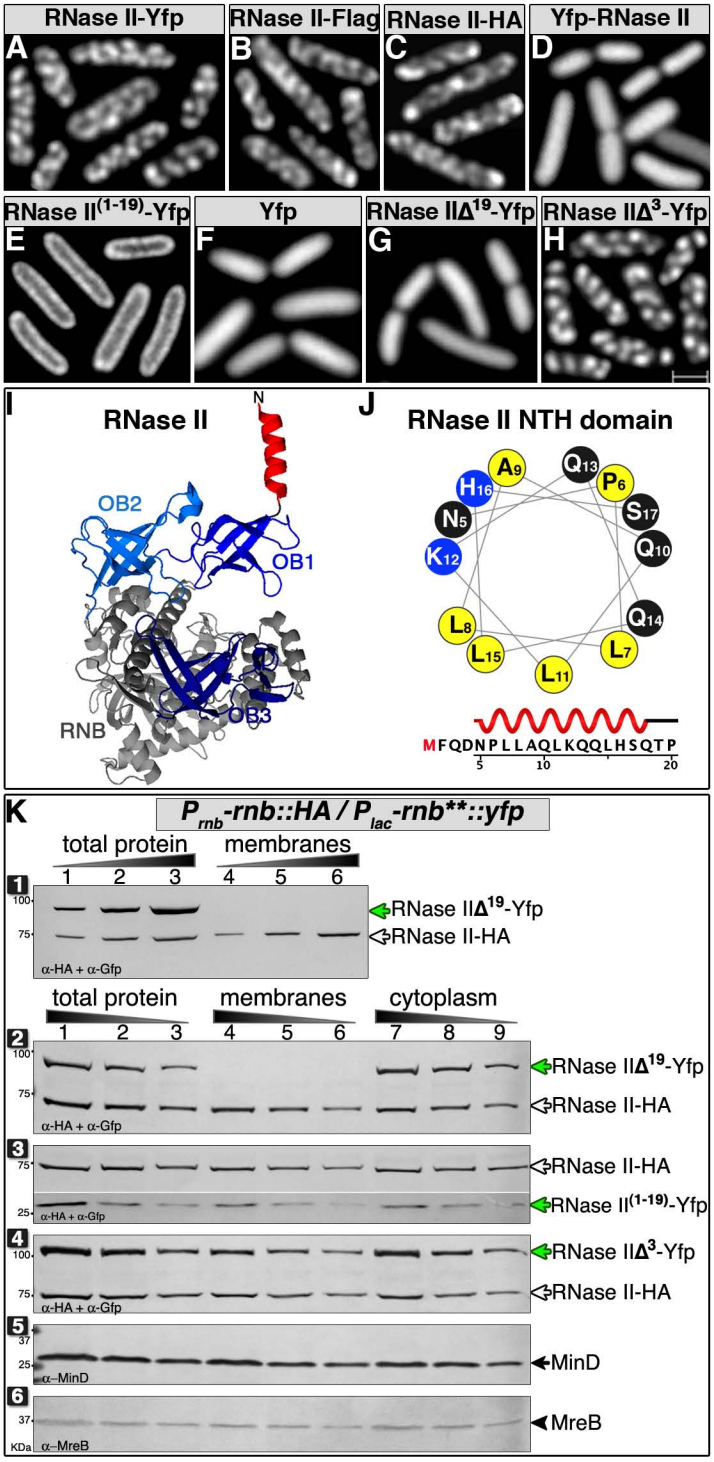

Figure 2

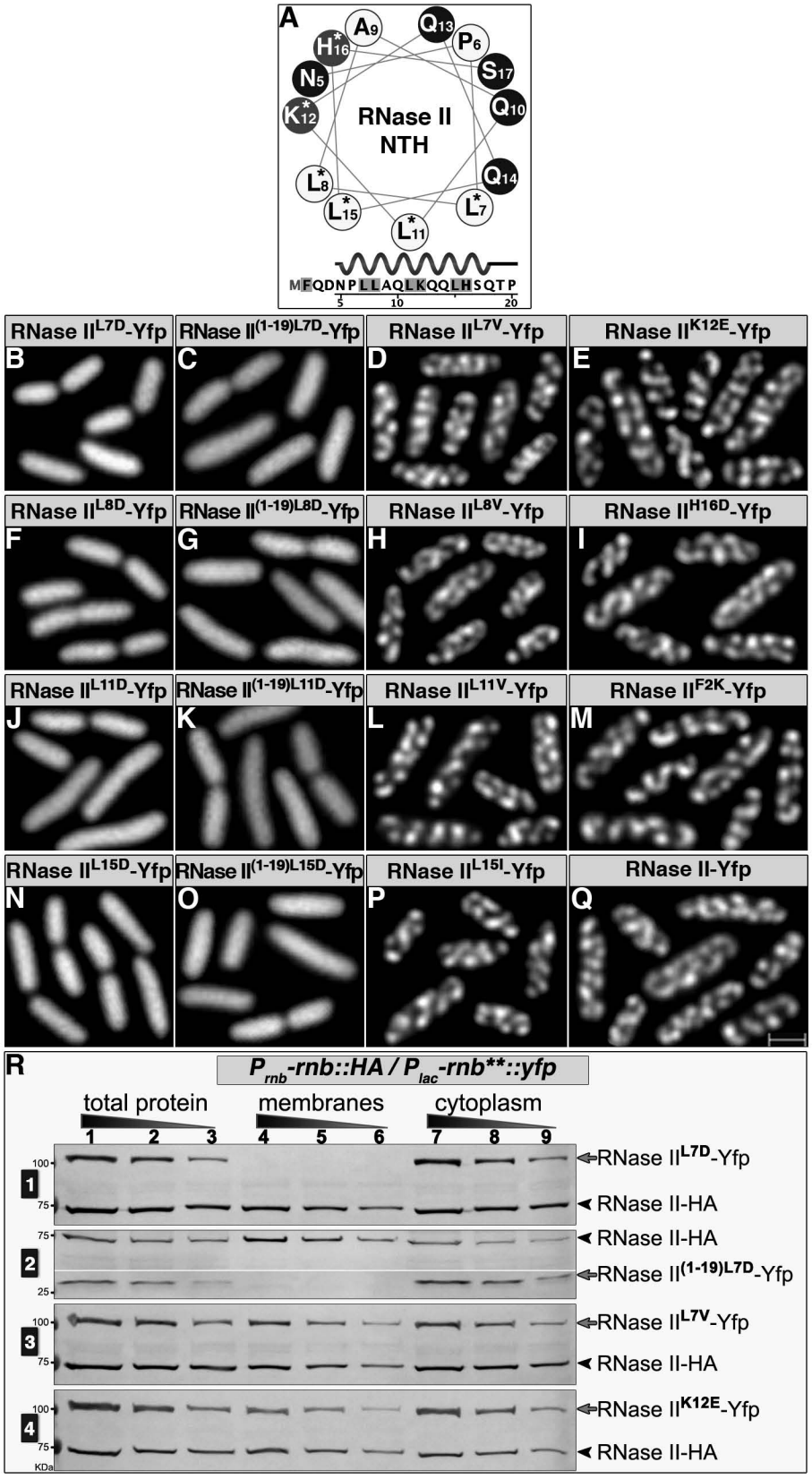

Figure 3

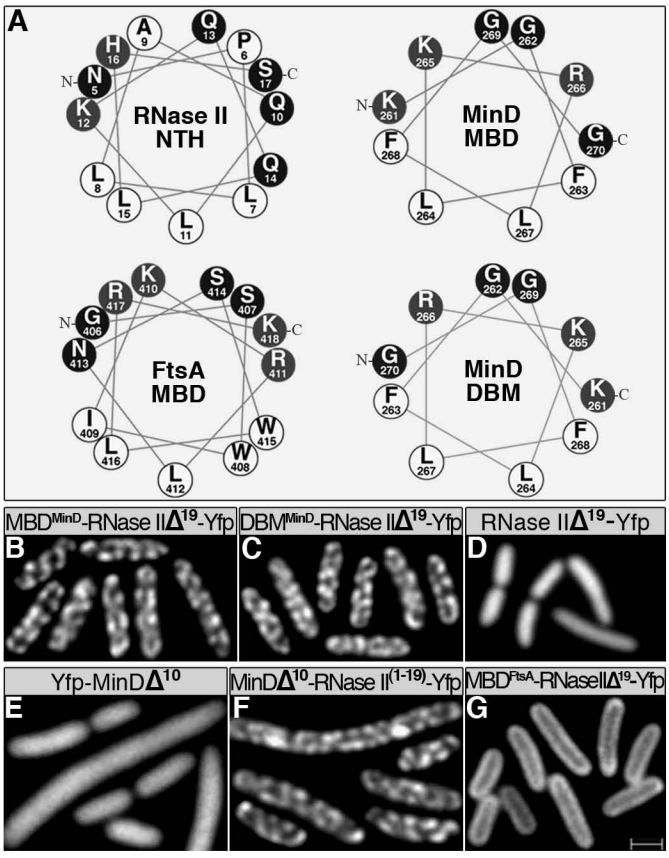

Figure 4

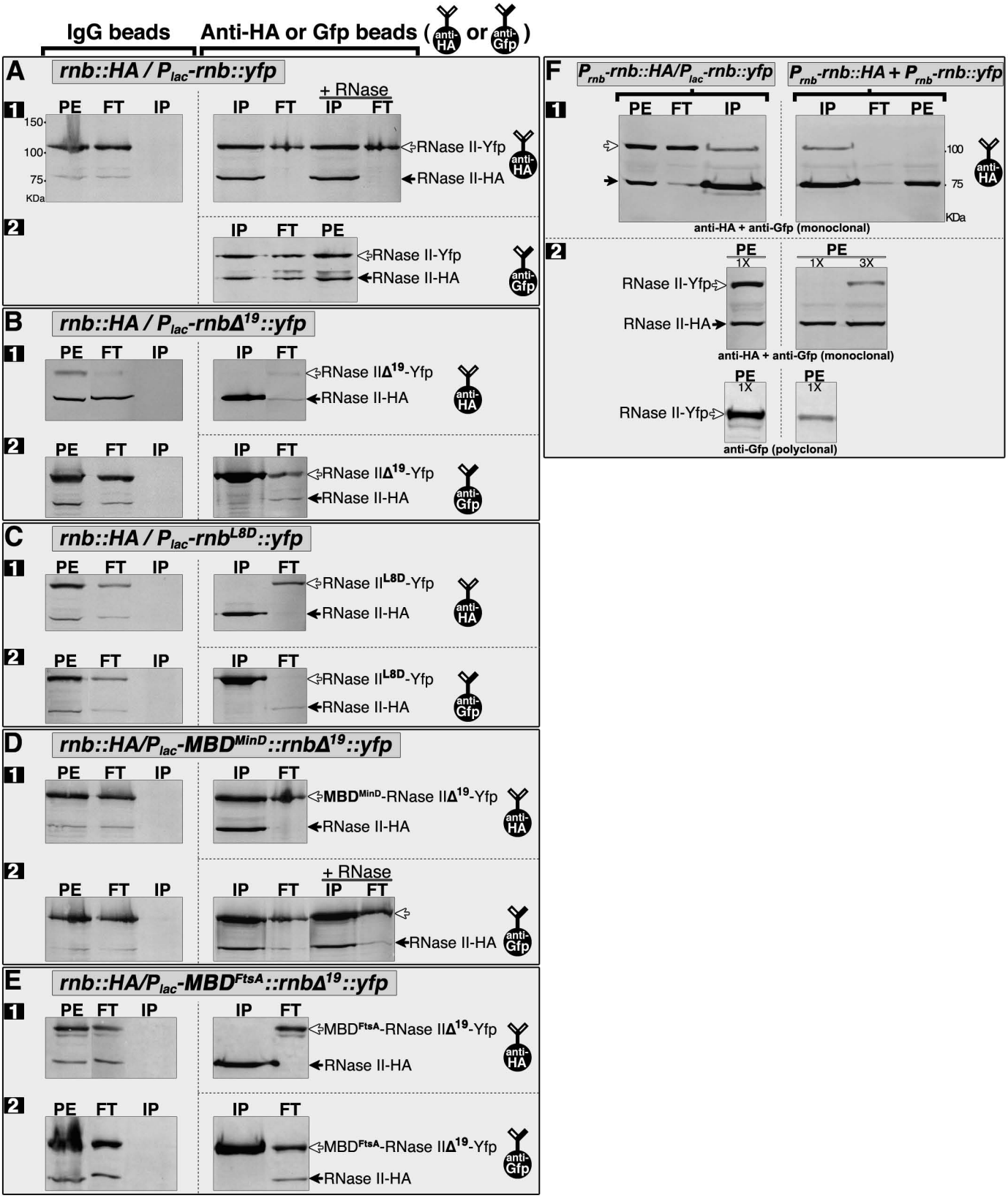

Figure 5